Relation of Eurasian Snow Cover and Indian Summer Monsoon Rainfall: Importance of the Delayed Hydrological Effect

SUBHADEEP HALDER AND PAUL A. DIRMEYER

Center for Ocean–Land–Atmosphere Studies, George Mason University, Fairfax, Virginia

(Manuscript received 30 December 2015, in final form 5 October 2016)

ABSTRACT

This observationally based study demonstrates the importance of the delayed hydrological response of snow cover and snowmelt over the Eurasian region and Tibet for variability of Indian summer monsoon rainfall during the first two months after onset. Using snow cover fraction and snow water equivalent data during 1967–2003, it is demonstrated that, although the snow-albedo effect is prevalent over western Eurasia, the delayed hydrological effect is strong and persistent over the eastern part. Long soil moisture memory and strong sensitivity of surface fluxes to soil moisture variations over eastern Asia and Tibet provide a mechanism for soil moisture anomalies generated by anomalies in winter and spring snowfall to affect rainfall during the initial months in summer. Dry soil moisture anomalies over the eastern Eurasian region associated with anomalous heating at the surface and midtroposphere help in anchoring of an anomalous upper-tropospheric ‘‘blocking’’ ridge around 100°E and its persistence. This not only leads to prolonged weakening of the subtropical westerly jet but also shifts its position southward of 30°N, followed by penetration of anomalous troughs in the westerlies into the Indian region. Simultaneously, intrusion of cold and dry air from the midlatitudes can reduce the convective instability and hence rainfall over India after the onset. Such a southward shift of the jet can also significantly weaken the vertical easterly wind shear over the Indian region in summer and lead to decrease in rainfall. This delayed hydrological effect also has the potential to modulate the snow–atmosphere coupling strength for temperature and precipitation in operational forecast models through soil moisture–evaporation–precipitation feedbacks.

1. Introduction

Snow cover plays a significant role in Earth's climate system (Xu and Dirmeyer 2011) and is a potential source of predictability (Douville 2010). Snow–atmosphere coupling manifests in two ways: an instantaneous albedo effect (Dickinson 1983; Hall et al. 2008) and a delayed hydrological effect (Cohen and Rind 1991; Xu and Dirmeyer 2013a,b). The albedo effect directly influences absorbed surface radiation and thereby alters turbulent fluxes, surface temperature, and the density and temperature of air by diabatic heating/cooling. It also depends on the availability of shortwave insolation; hence, the albedo effect should become stronger as winter progresses into spring. On the other hand, soil moisture anomalies generated from snowmelt during the spring can modulate land–atmosphere coupling (Xu and Dirmeyer 2011) and act as a delayed snow-driven feedback with the atmosphere into summer.

Besides the positive feedback due to snow albedo (Wiscombe and Warren 1980; Xu and Dirmeyer 2013a), there is also a negative feedback due to snowfall–atmospheric stability relationships (Walland and Simmonds 1996) that is self-regulating in nature. In certain high-latitude regions in winter, the lower-tropospheric temperature may decrease with a sudden increase in snow cover, leading to increased static stability and unfavorable conditions for further snowfall. Sublimation and redistribution by wind would further reduce the snow amount. However, the ensuing increase in sensible heat fluxes and reduction in stability would create conditions suitable for snowstorms and increased snow cover once again. Processes such as snow sublimation, compaction, melting, and generation of runoff are highly nonlinear and complicated. Even more, their representation in climate models is not accurate (Niu and Yang 2006). Despite these shortcomings, the importance of snow hydrological effects in determining the land–atmosphere coupling during winter and spring has been demonstrated in a climate model by Xu and Dirmeyer (2011, 2013b) with potential relevance to the

Corresponding author e-mail: Subhadeep Halder, shalder3@gmu.edu

DOI: 10.1175/JCLI-D-16-0033.1

established inverse relationship Eurasian snow cover has with the Indian summer monsoon (Turner and Slingo 2011; Saha et al. 2013).

The largest spatiotemporal variability in snow is observed over the Eurasian continent. Blanford (1884) was among the first to identify an inverse relationship between winter snow and summer monsoon rainfall over India. Thereafter, numerous observational studies have investigated the inverse relationship between Eurasian snow and Indian summer monsoon rainfall (ISMR) during June–September (JJAS; e.g., Hahn and Shukla 1976; Dey and Bhanukumar 1982; Dickson 1984; Ropelewski et al. 1984; Dey et al. 1985; Shukla and Mooley 1987; Khandekar 1991; Parthasarathy and Yang 1995; Sankar-Rao et al. 1996; Yang 1996; Bamzai and Shukla 1999; Kripalani and Kulkarni 1999; Xu et al. 2009). Several modeling studies have also investigated the mechanisms underlying this relationship (e.g., Shukla 1984; Barnett et al. 1988; Vernekar et al. 1995; Douville and Royer 1996; Dong and Valdes 1998; Bamzai and Marx 2000; Gong et al. 2004; Dash et al. 2005; Turner and Slingo 2011; Saha et al. 2013). It is imperative to state that, although the actual domain demarcated to be the Eurasian region is quite variable in all these studies, the mechanism being explored based on snow-albedo effect has been the same.

Some studies based on statistical analysis (e.g., Shinoda 2001; Robock et al. 2003; Peings and Douville 2010) have questioned the validity of this teleconnection and argued that it is modulated strongly by the El Niño–Southern Oscillation (ENSO)–ISMR relationship. Meehl (1994) suggested that surface temperature anomalies over Eurasia and South Asia are controlled by changes in large-scale midlatitude circulation that are, in turn, driven by convective heating anomalies associated with the tropical biennial oscillation (TBO). Fasullo (2004) found the relationship between Eurasian snow cover and rainfall mainly over northern parts of India to be stronger during neutral ENSO years. Despite that, modeling studies (Ferranti and Molteni 1999; Turner and Slingo 2011) have proved that this relationship holds independent of the ENSO–ISMR relationship. Senan et al. (2016) have further shown that positive snow depth anomalies over the Himalayan–Tibetan Plateau region in early April can delay the onset of the monsoon. However, none of the above studies have investigated in detail the impact the delayed hydrological feedback associated with snowmelt has on the snow–atmosphere coupling over the Eurasian region and the variability of the ISMR on subseasonal time scales or its inherent mechanisms. Buermann et al. (2005), using statistical techniques, did hypothesize on the role of springtime surface conditions as a probable ''bridge'' between the wintertime Arctic circulation and summer monsoon rainfall during June, but they concentrated more on the northwest part of India. It needs to be thoroughly investigated whether anomalous circulation changes associated with changes in surface hydrology over the Eurasian region could also affect the ISMR variability on subseasonal time scales and whether persistence in land surface states can induce and/or prolong reduced rainfall activity.

The Indian summer monsoon season from June to September is characterized by strong intraseasonal rainfall variability (Sikka and Gadgil 1980; Krishnamurthy and Shukla 2000; Goswami 2007) in the form of epochs of above- or below-normal rainfall activity termed as ''active'' and ''break'' periods, respectively. These intraseasonal variations in rainfall also contribute to the interannual variability of all-India seasonal rainfall (Goswami 2007). Extended periods of active or break situation in terms of rainfall can lead to flooding or drought conditions, causing damage to agriculture, human life, and property. For example, sufficient soil moisture is required in order to grow paddies of rice (one of the staple kharif crops) and later sowing over most parts of India during May–July. Furthermore, the rainfall received over India in summer also affects regional economies (Kumar et al. 2011). Hence, accurate prediction of the subseasonal variability of rainfall is highly important to agriculture and flood forecasts (Sahai et al. 2015). The variability and predictability of ISMR on subseasonal and seasonal time scales are governed by slowly varying boundary conditions, such as sea surface temperature (SST) (Delsole and Shukla 2012), snow cover (Saha et al. 2013; Senan et al. 2016), soil moisture (Saha et al. 2011, 2012; Rai et al. 2015), and associated land–atmosphere feedbacks (Halder et al. 2015) and land use/land cover changes (Halder et al. 2016). Internal atmospheric dynamics have also been shown to govern about half of the interannual variability (Goswami and Xavier 2005). Therefore, skillful prediction of the ISMR not only depends on the accuracy of the initial and boundary conditions but also on the proper representation of land–ocean–atmosphere coupled interactions in dynamical models. The impact of spring snow cover and snowmelt on subseasonal rainfall variability in the form of break situations over India, particularly during June–July when the influence of El Niño/La Niña is suggested to be weak (Rai et al. 2015), has not been investigated so far.

In this paper, we demonstrate the impact of the delayed hydrological response of snow cover and snowmelt over eastern Eurasia in the variability of ISMR during the first two months (30- and 60-day averaged periods) after onset. Based on our analysis, we propose a hypothesis that explains how soil moisture anomalies over the eastern Eurasian region can play a role in reducing or enhancing rainfall activity over the Indian region during the first two months after onset through land–atmosphere feedbacks. The paper is organized as follows. Data and methodology are described in detail in section 2. Observed climatology and variability of snow cover fraction and snow water equivalent during winter and spring and their changes associated with rainfall after the onset of monsoon are discussed in sections 3a and 3b. Our hypothesis related to the mechanism of changes in post-onset rainfall is proposed in section 3c. Furthermore, the delayed hydrological effect associated with snowmelt and characteristics of land–atmosphere coupling over the Eurasian region is described in section 3d. Finally, conclusions are summarized in section 4.

2. Data and method

We have used high-resolution (0.5° × 0.5°) daily gridded rainfall from the Asian Precipitation–Highly Resolved Observational Data Integration Toward Evaluation of Water Resources (APHRODITE) (Yatagai et al. 2012) for the 37 years 1967–2003. Northern Hemisphere monthly gridded 2° × 2° snow cover fraction (SCF) data for the same period as described in Robinson (1993) and Robinson and Frei (2000) have been used for understanding its variability during winter and spring. Apart from that, Global Land Data Assimilation System, version 2.0, (GLDAS-2.0) daily snow water equivalent (SWE), latent and sensible heat fluxes, and soil moisture [surface (0–10 cm) and subsurface (10–40 cm)] analyses for 1967–2003 at 1° × 1° resolution are used (Rodell et al. 2004).

We have defined average SCF and SWE for the months December–January (DJ) to represent winter, February–March (FM) to represent the transition from winter to spring, and April–May (AM) to represent late spring conditions for our study. The climatological mean date of onset of the Indian summer monsoon over the southern tip of the state of Kerala is 1 June, as defined by the India Meteorological Department. However, there is considerable interannual variability in the onset date. For this study, we analyzed the post-onset variation of rainfall over the Indian monsoon region by averaging rainfall during the first 30 days after onset (30DAO) and first 60 days after onset (60DAO). For that purpose, we have used observed onset dates of the Indian summer monsoon reported by Pai and Rajeevan (2009). The 60DAO period captures the rainfall variability mostly during June and July, and some part of August during years when the onset is late.

For the analysis of near-surface variables, we have used monthly 2-m temperature (0.5° × 0.5°) from the Climate Research Unit of the University of East Anglia (Harris et al. 2014) for the period 1967–2003. We have used daily values of planetary boundary layer height (HPBL) simulated using the global coupled model Climate Forecast System, version 2, (CFSv2) of the National Centers of Environmental Prediction (Saha et al. 2014) at T126L64 resolution. For that purpose, the model is initialized at 0000 UTC 1 April every year from 1982 until 2003, using the CFS reanalysis (Saha et al. 2010) and run until 1800 UTC 1 October. The atmospheric model is coupled to the Modular Ocean Model, version 4, (MOM4) (Griffies et al. 2004) and the Noah land surface model (Ek et al. 2003), version 2.7.1, which is also the model used in GLDAS-2.0. Apart from that, monthly geopotential height, temperature and zonal and meridional wind (~1.4° × 1.4°) at multiple pressure levels from ERA-40 (Uppala et al. 2005) have been used for the period 1967–2002 for the analysis of upper-atmospheric features. To account for the spatial variability in soil and vegetation types used in GLDAS-2.0, soil wetness index (SWI) values are calculated by scaling the soil moisture using porosity and wilting points of each soil type. Significance for differences in the mean is tested based on a Welch's *t* test, which is a Student's *t* test for unequal sample sizes and variance.

3. Results

a. Observed SCF and SWE over Eurasia

Figure 1 shows the mean SCF and SWE averaged during DJ (top row), FM (middle row), and AM (bottom row) and their interannual standard deviations for the period 1967–2003. SCF is the main factor controlling the snow-albedo effect. During winter, northern parts of Eurasia and western and southeast Tibet are completely covered by snow. Snow cover is also evident south of the Caucasus and the western part of the plateau of Iran. There is little interannual variability north of 50°N, implying complete snow cover. However, southern Eurasia has large interannual variability along a zonal band bounded mostly between 30° and 55°N, where snow becomes more ephemeral. There is weak (strong) variability in snow cover over western (eastern) Tibet, which means that snow cover is more (less) continuous there. During the transition from winter to spring (FM), the mean SCF changes little, but increased snowmelt, greater solar radiation, and feedbacks discussed above contribute to enhanced variability over western and southern Eurasia, including Tibet. During late spring (AM), the edge of permanent snow cover has receded

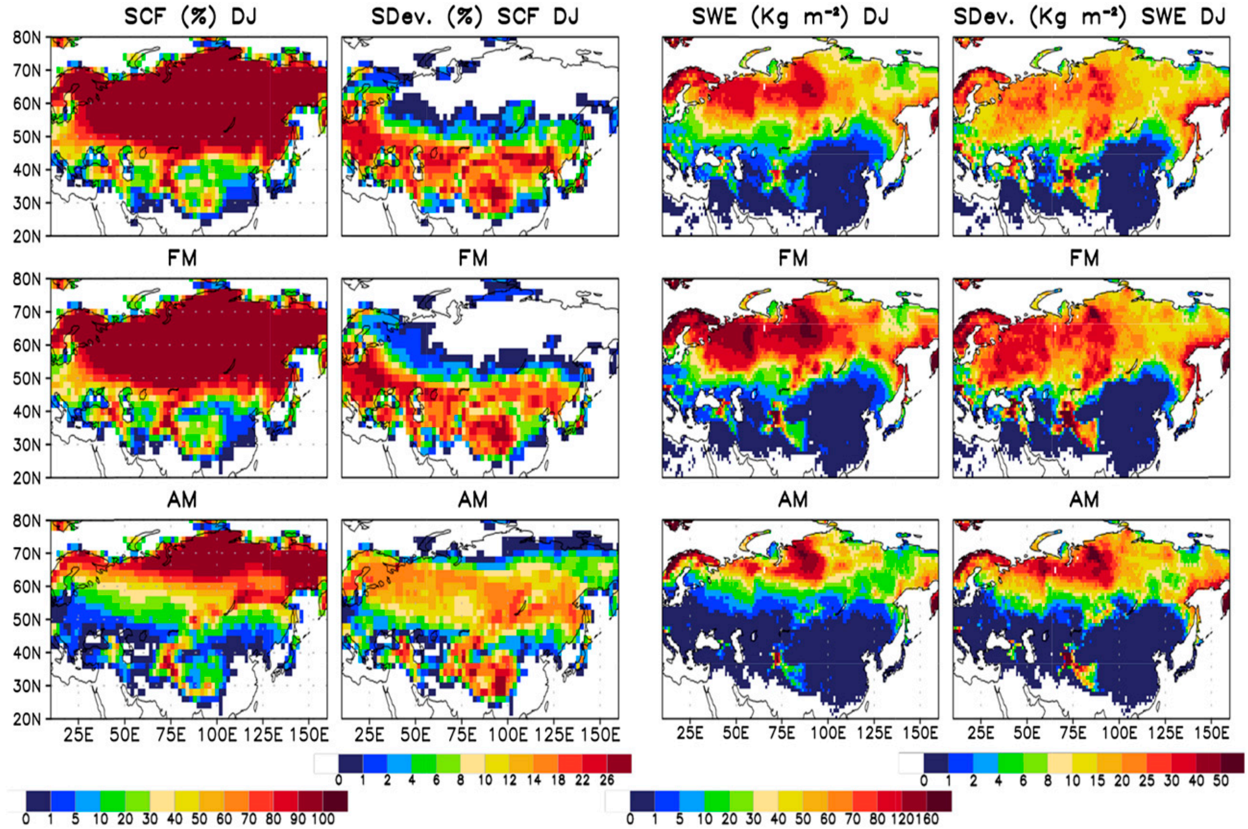

FIG. 1. (left) Mean and (center left) interannual std dev of NOAA/NESDIS monthly SCF (%) averaged during (top) DJ, (middle) FM, and (bottom) AM from 1967 until 2003. (center right),(right) As in (left) and (center left), but for monthly GLDAS-2.0 SWE (kg m^{-2}).

farther north. There is enhanced variability between 45° and 70°N and over Tibet. This is the period when snow hydrological processes and the albedo effect start working in tandem over this latitudinal belt and may increase the snow–atmosphere coupling strength, affecting surface and atmospheric parameters close to the ground. Western Tibet still remains covered with snow because of its altitude and colder temperatures.

SWE (kg m^{-2}) is a measure of water mass in the snowpack. It is the characteristic that determines the potential for the snow hydrologic effect. From Fig. 1 it is evident that snow cover in winter (DJ) is relatively deep over the region north of 50°N and west of 100°E, apart from western Tibet and the Himalayas and the eastern Eurasian edge. These areas and parts of eastern Siberia have large interannual variability as a result of freezing/thawing of snow. During FM, there is an increase in the water content of the snowpack and its interannual variability as well that may enhance the snow hydrologic effect. By AM, the area with large SWE retreats farther north but still shows strong interannual variability north of 50°N. Western Tibet and the Himalayas demonstrate strong interannual variability even in late spring, which could possibly affect the surface temperature and diabatic heating of the atmosphere through the snow hydrological effect. The retreat over the western part of Eurasia appears to be faster than that over the eastern part, which could be attributed to warm temperature advection over that region (Thompson and Wallace 2000). As a result, there is a slight northwest–southeast tilt in the spatial pattern of maximum SCF and SWE during AM.

b. *Variability of post-onset rainfall over India and its relation with SCF and SWE*

The mean onset date of the Indian summer monsoon during the period 1967–2003 is 2 June, with an interannual standard deviation of 7.5 days [based on data from Pai and Rajeevan (2009)]. Average rainfall during the 30DAO period shows maxima over the Western Ghats, the hilly terrain of the eastern parts of central India (CI; 16.5–26.5°N and 74.5–86.5°E), east and northeast India, and the foothills of the Himalayas (Fig. 2). The rain-shadow region over peninsular India and the drier northwestern areas are also evident. Rainfall further increases in intensity during the 60DAO period over these places and particularly over central

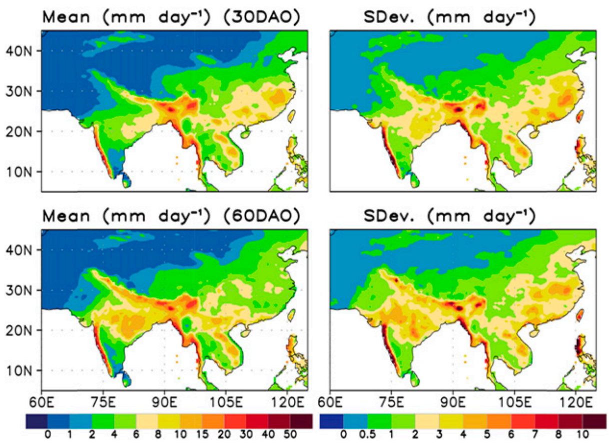

FIG. 2. Mean rainfall from APHRODITE and interannual std dev (SDev.) (mm day^{-1}) averaged during (top) the 30DAO and (bottom) 60DAO periods of monsoon, from 1967 until 2003.

India, covering more parts of western India and its northwest primarily because of an increase in rainfall in July. Interannual variability follows the mean spatial pattern but shows greater spatial coverage and magnitude during the 60DAO period. Kothawale and Kulkarni's (2014) analysis using observed data for over 100 years suggests that, during the period 1967–2003, there were about 6 years when the all-India rainfall departure during June, July, or June plus July exceeded 10% of the climatology, and that affected the seasonal total rainfall as well. The climatological mean and interannual standard deviation of rainfall averaged over the all-India domain during the 30DAO and 60DAO periods are captured very well by the statistics over CI (figure not shown). Therefore, we have chosen the CI domain in our study for further analysis of rainfall anomalies over India during these periods. There is a small but insignificant increasing trend in rainfall over the 37-yr period (figure not shown).

To understand the delayed hydrological effect of Eurasian snow on rainfall over India during the monsoon season, composites of SCF and SWE during DJ, FM, and AM of different years are prepared on the basis of standardized CI averaged rainfall anomalies during the 30DAO and 60DAO periods. An above- (below-) normal rainfall year for India is identified when the standardized CI averaged rainfall anomaly during 30DAO and 60DAO (1967–2003) is $\geq +1$ standard deviation (≤ -1 standard deviation). For simplicity, we will refer to these above- and below-normal rainfall years (6 in each case) as positive rainfall (POSRF) and negative rainfall (NEGRF) years, respectively. Figure 3 shows the difference (NEGRF $-$ POSRF) of SCF and SWE composites based on the NEGRF and POSRF years determined on the basis of rainfall anomalies during the 30DAO and 60DAO periods, for DJ (top row), FM (middle), and AM (bottom). Differences in SCF north of 50°N and east of 30°E between NEGRF and POSRF years are minimal during DJ or FM mostly because snow coverage is of a permanent nature over these areas during these months. Negative anomalies of SWE over a large part of western Eurasia suggest that snow depths are relatively thin during DJ and FM in the NEGRF years. There are at times positive anomalies of both SCF and SWE over Europe, western Russia, Kazakhstan, and areas north and northeast of Tibet. Positive anomalies of SCF over these areas during DJ and FM would increase the surface albedo and possibly affect the surface temperature gradient between the land and ocean and hence rainfall over India during the 30DAO and 60DAO periods. This supports earlier results shown for the entire June–September season (cf. Fig. 4a in Bamzai and Shukla 1999). However, it is also important to mention that the spatial pattern of surface temperature anomalies over the entire domain is too complex to speculate specifically on any resulting north–south land–ocean temperature gradient. Northern parts of Eurasia (north of 65°N, east of 75°E) also have positive SWE anomalies during DJ and FM for NEGRF years, suggesting increased snow depth. However, those changes are farther away from the tropics. On the other hand, south of 65°N and closer to India there is decreased SWE that may have a greater impact on all-India rainfall through changes in surface hydrology, fluxes, and near-surface temperature. There are some changes in sign of the anomalous SCF over southern Europe and western Russia during FM that may be induced by atmospheric wave activity suggested in earlier studies (Thompson and Wallace 2000).

During AM there are positive (negative) SCF anomalies over western (eastern) Eurasia. However, SWE anomalies suggest that the snow depth is higher mostly over northern Europe, northern and extreme eastern Eurasia, and south of 50°N over western Eurasia. Although SCF anomalies over western Eurasia (45°–65°N, 30°–80°E) during NEGRF years are higher than during POSRF years, the snow depths are relatively thin. These positive anomalies, through the snow-albedo effect, may also decrease the land–ocean temperature gradient and affect the all-India rainfall adversely. However, the snow-albedo effect during AM for NEGRF years would be short lived, as the SWE is found to be relatively less than during POSRF years. We also note that there is a significant decrease in SCF as well as SWE in many areas over eastern Eurasia, around Mongolia, and eastern China (35°–60°N and 85°–125°E). However, changes in SWE extend farther toward the south. The entire region over eastern Eurasia south of 60°N happens to be arid to semiarid, with less soil moisture (cf. Fig. 4) but ample net

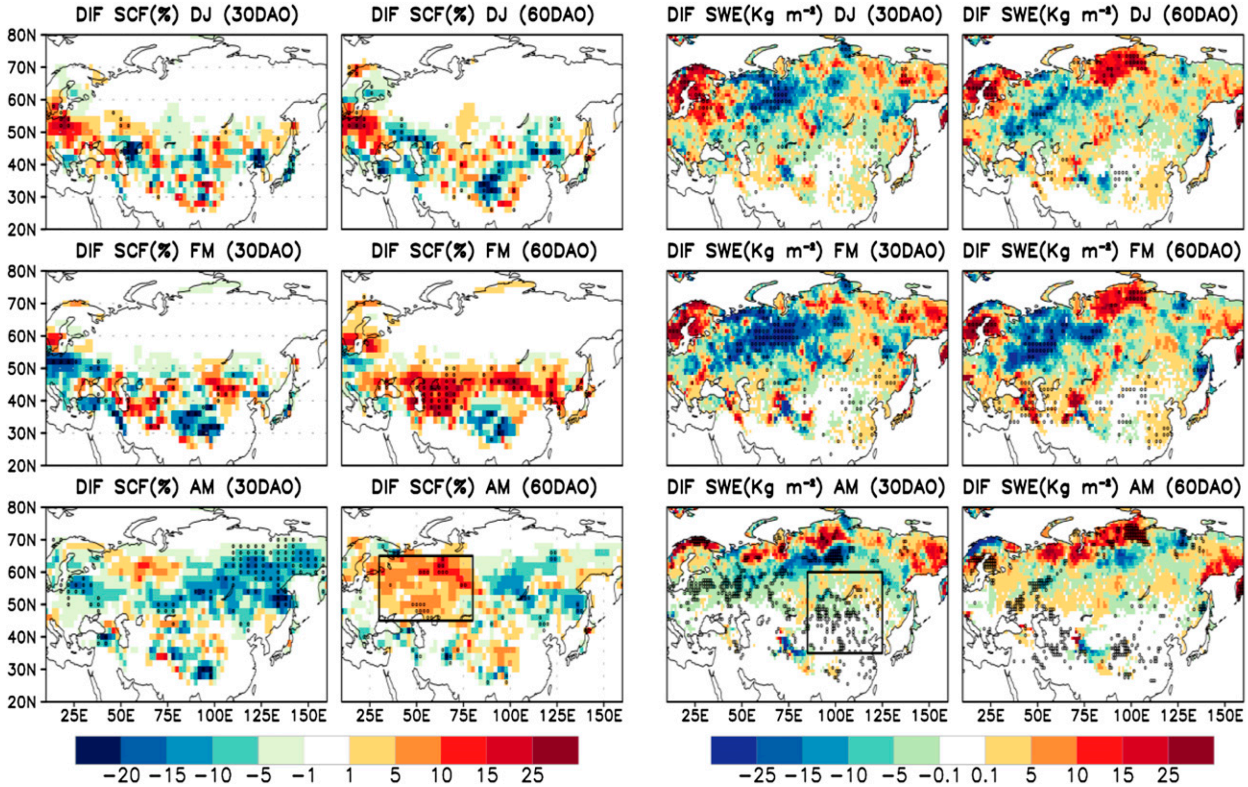

FIG. 3. Mean difference (NEGRF − POSRF years) of NOAA/NESDIS SCF based on NEGRF and POSRF years identified from standardized anomalies of CI averaged rainfall from APHRODITE during 1967–2003 for the (left) 30DAO and (center left) 60DAO periods of Indian summer monsoon. The differences (%) are shown during (top) DJ, (middle) FM, and (bottom) AM. (center right), (right) As in (left) and (center left), but for GLDAS-2.0 SWE (kg m^{-2}). Stippled areas denote differences significant at the 90% confidence level. The western and eastern Eurasian boxes are enclosed in black lines.

radiation (figure not shown), which implies that it is more moisture limited and not radiation limited. Anomalous soil moisture changes resulting from snowmelt would shift the land–atmospheric conditions from that of a dry to that of a transitional regime and result in profound sensitivity of the surface fluxes of heat and moisture, unlike in western Eurasia. Therefore, although changes in SWE (and hence associated soil moisture anomalies) are small, they are expected to create large changes in surface moisture and heat fluxes (further shown in section 3d). As an aside, it may be noted that the eastern Eurasian region around Mongolia is important both in terms of snow–atmosphere coupling (Xu and Dirmeyer 2011, 2013a,b) and soil moisture–atmosphere coupling (Koster et al. 2004), although the multimodel averaged coupling strength was reported to be weaker than in other global hot spots. During the entire winter and spring seasons (DJ, FM, and AM), negative anomalies of SCF and SWE are mostly observed over the Himalayan range and Tibetan region during NEGRF years as compared to POSRF years. Although this may suggest a positive association with all-India rainfall in the post-onset period (mostly during June and July) the changes are not significant. Differences in composites based on early and late monsoon onset years during the period 1967–2003 (figure not shown) suggest there is a significant increase in SCF and SWE over the western Himalayas and Tibet when the onset is late. This relationship has also been investigated through modeling experiments (Senan et al. 2016). In the following sections, differences in hydrological properties between these two regions and their effect on other surface and atmospheric variables are explored.

c. *Changes in surface and upper-atmospheric parameters*

The climatology of surface soil moisture and 2-m near-surface air temperature during AM are analyzed at first (Fig. 4, top row). Mean surface soil moisture is high across Eurasia (north of 55°N, west of 130°E), the western Himalayas, west of the Caspian Sea (all areas where SWE variability is high; Fig. 1), and East Asia. Areas over Tibet and the Gobi Desert around Mongolia and China are relatively dry. Surface temperatures are

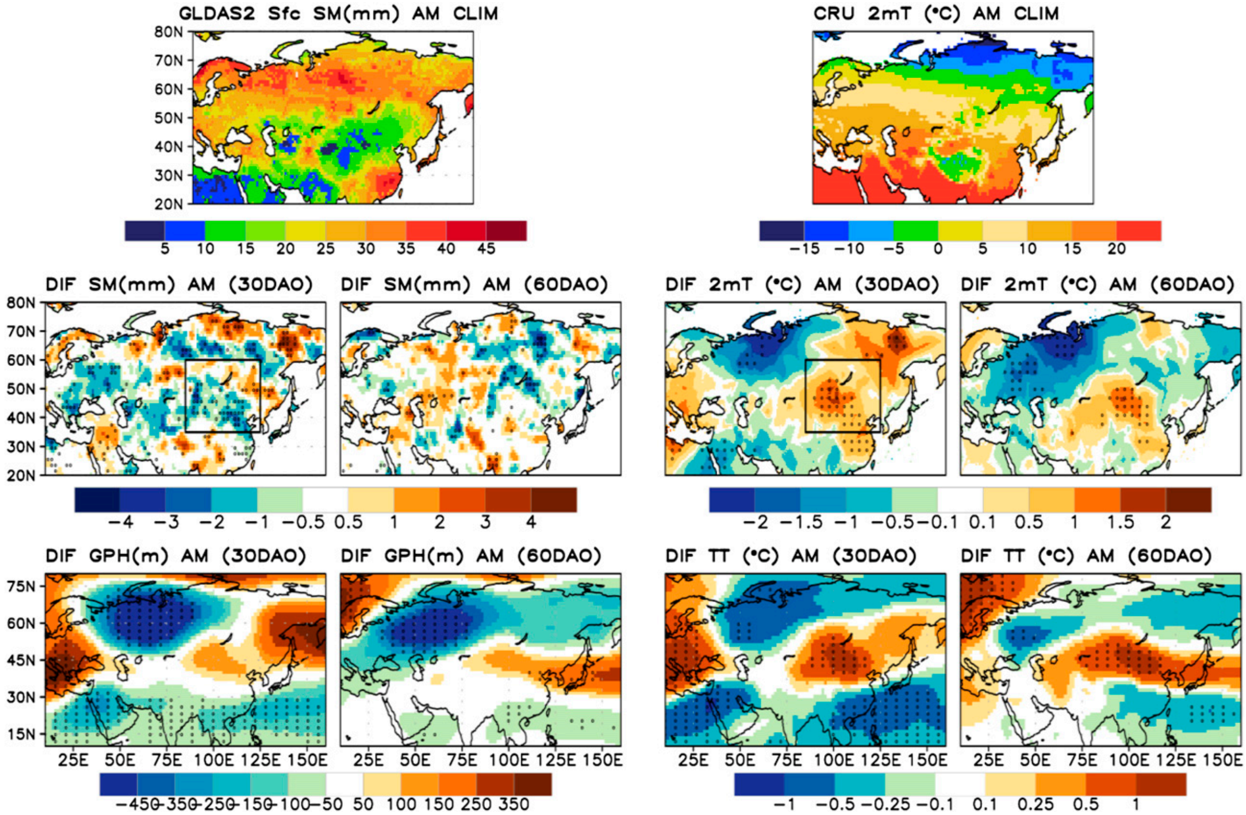

FIG. 4. Mean (top left) GLDAS-2.0 surface soil moisture (0–10 cm; mm) and (top right) CRU Time Series (TS3.21) 2-m temperature (K) during 1967–2003. (middle left), (middle right) Differences only during AM calculated as in Fig. 3, for (middle left) GLDAS-2.0 surface soil moisture (mm) and (middle right) CRU TS3.21 2-m temperature (K). (bottom left), (bottom right) Similar differences during AM based on (bottom left) ERA-40 geopotential height (GPH; m) and (bottom right) tropospheric temperature (TT; K) averaged between 700 and 400 hPa. Stippled areas denote differences significant at the 90% confidence level. The eastern Eurasian box is enclosed in black lines.

freezing over the extreme northeast of Eurasia, as areas north of 60°N are still covered with snow, and the Tibetan Plateau. South of 40°N, surface temperatures are relatively warm. The difference between the composites of NEGRF and POSRF years shows a significant decrease in surface soil moisture over the eastern Eurasian box (35°–60°N, 85°–125°E,) enclosed in black lines and parts of western Eurasia. Associated with such drying (moistening) at the surface and changes in surface moisture fluxes (figure not shown), there is a significant increase (decrease) in 2-m air temperature. Decreased surface temperature over a large part of western Eurasia (between 25° and 80°E) and the northwest of India are indicative of a decreased land–ocean temperature gradient that affects the Indian monsoon adversely during NEGRF years. This is a well-known hypothesis (decrease in surface temperature due to the snow-albedo effect) that has been already proposed and tested in earlier studies. However, the hydrological effect associated with changes in SWE has not been investigated so far, at least in modeling studies, because of suspicion over the physical realism of the hydrological aspect of the land surface models employed in GCMs. Perhaps it is also a reason why the multimodel averaged coupling strength was noted to be weaker over the Eurasian region than over other global hot spots (Koster et al. 2004). We further note that such a decrease in surface temperature during NEGRF years, particularly to the north of India, is stronger during the 30DAO period than during 60DAO. This suggests that the hydrological effect associated with SWE changes may also be stronger during that period. It is interesting that, associated with warming (cooling) at the surface centered over Mongolia, there is also a significant warming (cooling) in the midtropospheric temperature averaged between 700 and 400 hPa. Apart from that, there is also an increase (decrease) in 500-hPa geopotential height associated with warming (cooling) over that region, but changes are not significant, unlike over western Eurasia. Nevertheless, this indicates the deep barotropic nature of the changes in the atmosphere associated with the surface changes.

To understand the impact of eastern Eurasian hydrology on the post-onset changes in Indian monsoon rainfall, changes in large-scale circulation are further analyzed using composite analyses based on soil moisture over the eastern Eurasian region. A time series of surface soil moisture anomalies during AM averaged over the eastern Eurasian box is prepared for the period 1967–2003. The anomalies are normalized by the standard deviation of the time series and detrended. Based on this, years are identified as positive soil moisture (POSSM) [negative soil moisture (NEGSM)] when the normalized anomalies are $\geq +1$ standard deviation (≤ -1 standard deviation). The resultant number of years is 6 in each case. The climatology of 200-hPa wind from ERA-40 (1967–2002) during AM and the difference between NEGSM and POSSM years are analyzed (Fig. 5, top row). Bottom panels in Fig. 5 show the same for 200-hPa wind composite in JJ and difference (NEGSM − POSSM years) based on standardized AM soil moisture anomalies.

The climatological location and strength of the subtropical westerly jet is evident around 30°N during AM, with easterlies south of 10°N over India. During JJ, the jet position moves farther northward around 40°N, easterlies take over its position over the Indian region, and the Tibetan anticyclone becomes evident near 25°N. Differences (NEGSM − POSSM) show that the core of the subtropical westerly jet shifts south of its normal position in AM during NEGSM years. Furthermore, the streamlines also suggest that anomalous troughs in the westerlies penetrate deep into the Indian region between 50° and 75°E during NEGSM years, possibly bringing dry and cold air into the Indian region and decreasing the convective instability (figure not shown) and, hence, the strength of the monsoon and rainfall (cf. Krishnan et al. 2009; Samanta et al. 2015). There is an anomalous anticyclone located to its northwest, a ridge toward its east located around 100°E, and an anomalous cyclonic circulation farther to the east over eastern China and Japan. The upper-level anticyclone east of India over Myanmar and Thailand (around 100°E) is associated with convection and rainfall activity over that region during May. That anticyclone is also found to extend to 60°N in the form of a ridge (a blocking ridge) and is centered over the eastern Eurasian box, which shows negative soil moisture anomalies and increased surface temperature. The upper-tropospheric blocking ridge around 100°E has been suggested to be responsible for preventing the eastward passage of troughs in the midlatitude westerlies [cf. Krishnan et al. (2009) and other references therein]. There are anomalous westerlies over the Indian region in the upper level, implying weakened easterlies. This is a classic example of the interaction of midlatitude waves with the Indian summer monsoon through upper-level circulation anomalies that is evident during certain long break situations on intraseasonal time scales (e.g., June and July) (Krishnan et al. 2000, 2009; Samanta et al. 2015). Differences in upper-level circulation during JJ composited on AM soil moisture anomalies also support this situation, the only difference being that the differences are slightly weaker. However, the location of the anomalous ridge around 100°E is in the same place during JJ, which suggests there is some persistence in the upper-level circulation features that are tied to the dry soil moisture anomalies over eastern Eurasia. So far, in none of the earlier studies had the role of soil hydrology over eastern Eurasia been identified in determining the position and duration of the blocking ridge.

Figure 6 is like Fig. 5, but for zonal (U) wind composites from 925–200 hPa, averaged between 50° and 80°E. The vertical distribution of mean zonal winds during AM shows westerlies north of 20°N and easterlies south of it that extend up to about 850 hPa (top row). During JJ, the subtropical westerly jet moves farther northward beyond 30°N, and the easterlies strengthen in the upper-atmospheric levels while surface westerlies emerge and strengthen over the Arabian Sea and northern Indian Ocean (bottom row). Furthermore, a strong vertical easterly shear of winds just north of the equator that is important for the northward propagation of the intertropical convergence zone (ITCZ), which brings in cloudiness and rainfall over the Indian region (Jiang et al. 2004) is evident. The difference between the composites of NEGSM and POSSM years during AM suggests that, when there are dry soil moisture anomalies over the eastern Eurasian region, there are anomalous upper-level westerlies north of the equator between 50° and 80°E and anomalous easterlies below. The strength of the subtropical westerly jet also decreases north of 30°N, and there is a southward shift in its position. This is further evident in the difference plot during JJ. Studies suggest that in normal monsoon years the subtropical westerly jet moves northward up to north of 30°N around the time of onset from May to June (cf. Soman and Krishna Kumar 1993). Furthermore, our analysis shows that the strength of the vertical easterly wind shear is significantly decreased during JJ in NEGSM years. The vertical easterly wind shear (the first baroclinic mode in the vertical) has been demonstrated to be important in maintaining the overall diabatic heating during the Asian monsoon (Webster and Yang 1992). These processes explain the dynamical mechanism through which the post-onset Indian

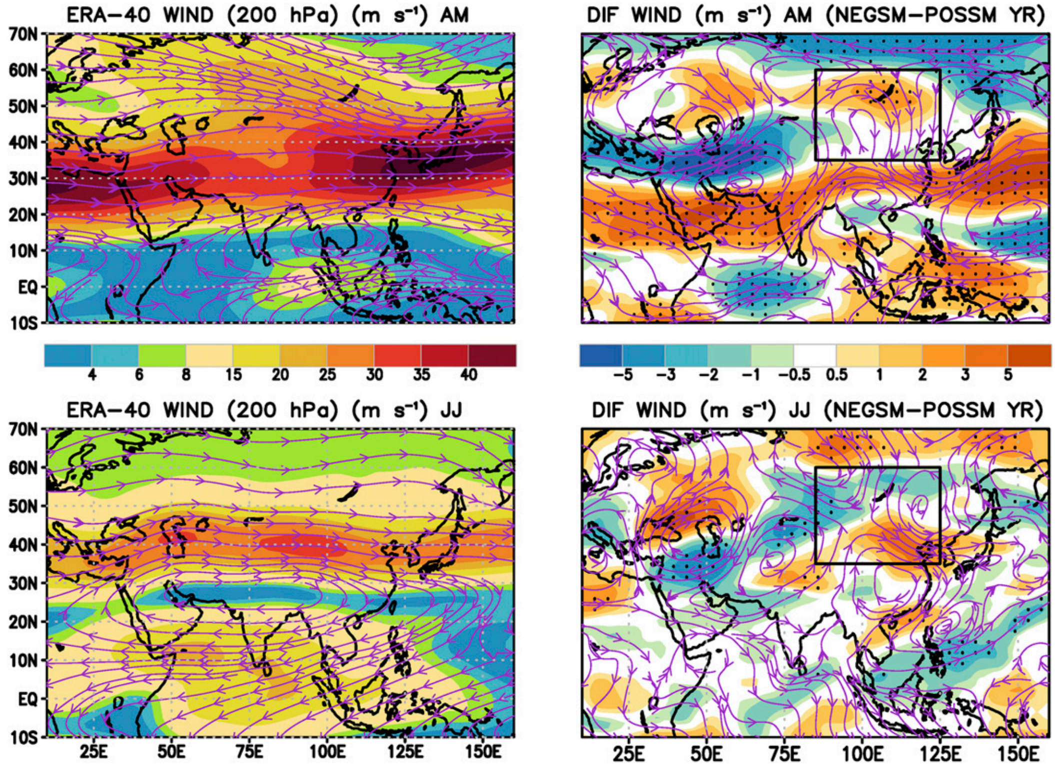

FIG. 5. Mean 200-hPa ERA-40 wind (m s^{-1}) during (top left) AM and (bottom left) JJ from 1967 until 2003. Shaded color shows the magnitude, and streamlines show the direction. Mean difference (NEGSM − POSSM years) of 200-hPa ERA-40 wind (m s^{-1}) during (top right) AM and (bottom right) JJ based on NEGSM and POSSM years identified from standardized anomalies of GLDAS-2.0 surface soil moisture in AM during 1967–2003. Stippled areas denote differences in magnitude of wind significant at the 90% confidence level. The eastern Eurasian box is enclosed in black lines.

summer monsoon rainfall is decreased along with anomalous soil moisture changes over eastern Eurasia. Conversely, wet soil moisture anomalies over the eastern Eurasian region would result in changes of opposite sign in the surface and upper-atmospheric variables, thus increasing rainfall activity after the onset of the Indian summer monsoon (figure not shown). In the following section, we further explore the surface hydrological characteristics over the Eurasian region and associated land–atmosphere coupling to understand the feedback between soil moisture and atmospheric variables.

d. Hydrological effect of snowmelt and associated sensitivity of surface fluxes

Memory of the snow anomalies persists in soil moisture states at the surface and subsurface and can contribute to the snow–atmosphere coupling strength after melting. To understand the difference in soil hydrological features between western and eastern Eurasia in terms of SWE and soil moisture, we first analyze their mean annual cycles and interannual variability (Fig. 7). For this, daily SWE and surface and subsurface soil moisture values are averaged over the western and eastern boxes. In all these figures, the solid line in the middle depicts the climatological mean, the long dashed lines bounding the mean show the interannual standard deviation, and the short dashed black lines show the range of maximum and minimum values. Over the western box, SWE attains its maximum by the end of February and thereafter rapidly decreases to zero by May. The variability is highest in April, which is also the time when the snow–atmosphere coupling strength is maximum (cf. Fig. 3 in Xu and Dirmeyer 2011). Over the eastern box, the mean and interannual variability are relatively less than for the western box. The maximum in SWE is attained during February; however, the decrease thereafter is more gradual. A decrease in SWE leads through snowmelt to a rapid increase in surface and subsurface soil moisture and variability over western Eurasia (Fig. 7, middle and bottom rows). Peak soil moisture is attained by early April, which is followed by a gradual decrease until July. However, the

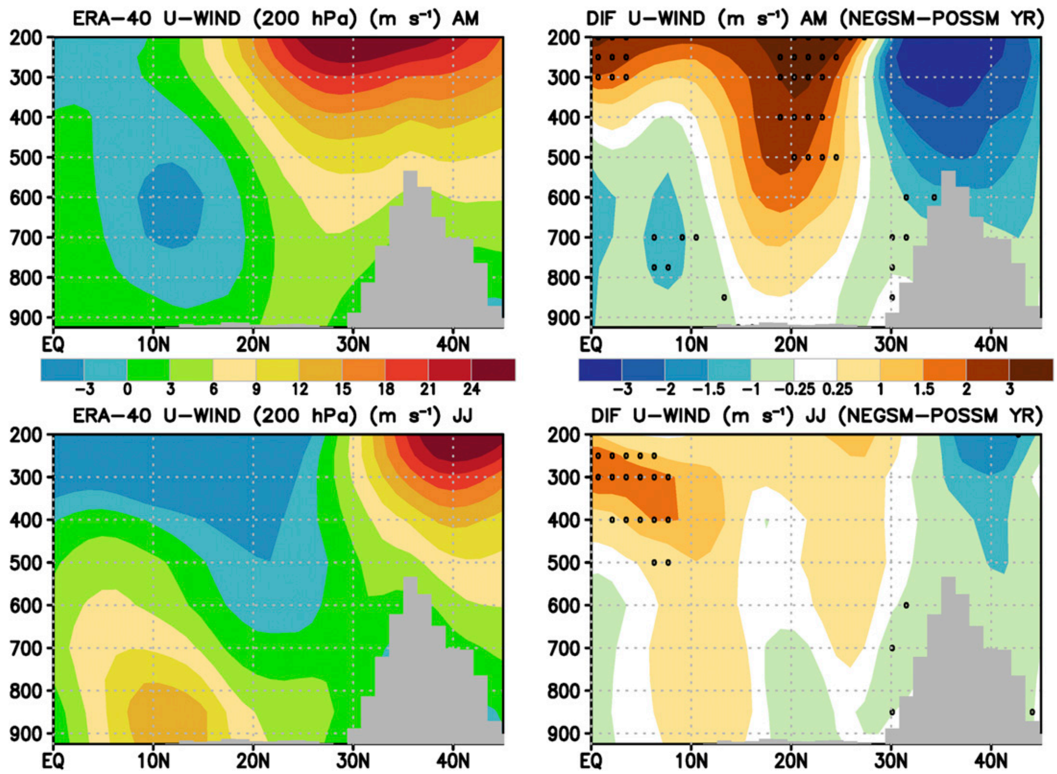

FIG. 6. As in Fig. 5, but based on 200-hPa ERA-40 zonal (U) wind (m s^{-1}) averaged between the longitudes 50° and 85°E. Stippled areas denote differences in magnitude of U-wind significant at the 90% confidence level.

variability is subdued compared to that in April. Another interesting feature is that the mean soil moisture in July is much lower than the driest values attained before April. Over the eastern box that is collocated with the Gobi Desert, soil moisture during spring is relatively less compared to the west. Interestingly, peak soil moisture values as well as strong interannual variability over the eastern box are attained one month later than in the west. Furthermore, mean soil moisture as well as its variability remain almost constant until mid May. There is a secondary peak in soil moisture over the eastern Eurasian region during June–August that could be attributed to local rainfall activity; however, the underlying reason is not investigated in the present study.

The implication of these differences between the west and the east is explored using land–atmosphere coupling metrics. Land–atmospheric coupling takes place via two legs: the terrestrial leg, where soil moisture affects surface fluxes of moisture and sensible heat (Dirmeyer 2011), and, second, the atmospheric leg, where variations in those fluxes affect the near-surface atmospheric variables, such as temperature, humidity, and boundary layer and its growth up to the lifting condensation level. Anomalous changes in surface and subsurface soil moisture can affect the near-surface atmospheric variables and possibly increase or decrease chances of triggering moist convection through the water or energy cycles (Dirmeyer et al. 2014) only if both the legs are in place. For that, strong sensitivity of the surface fluxes to soil moisture variations apart from variability is also required.

The area-averaged mean sensitivity of the surface latent heat flux (LHF) and sensible heat flux (SHF) to soil wetness variations over the western and eastern Eurasian boxes, respectively, are shown in the first two panels of Fig. 8 (top row) during April–July. Sensitivity is calculated from the slope of the linear regression of the fluxes on the soil wetness index (described in section 2). Furthermore, the sensitivities of surface fluxes are multiplied by the difference in mean monthly soil moisture anomalies during POSSM and NEGSM years over each box in order to depict the contrast. It is evident that the sensitivity of surface LHF and SHF is much stronger over the eastern box than over the west, at least until June. It is further interesting to note that sensitivity of LHF over the western box is negative during AM, which means that LHF variations are not controlled by soil moisture variations but by availability of net radiation and atmospheric demand. Therefore, the terrestrial leg of coupling is not in place. For the atmospheric leg,

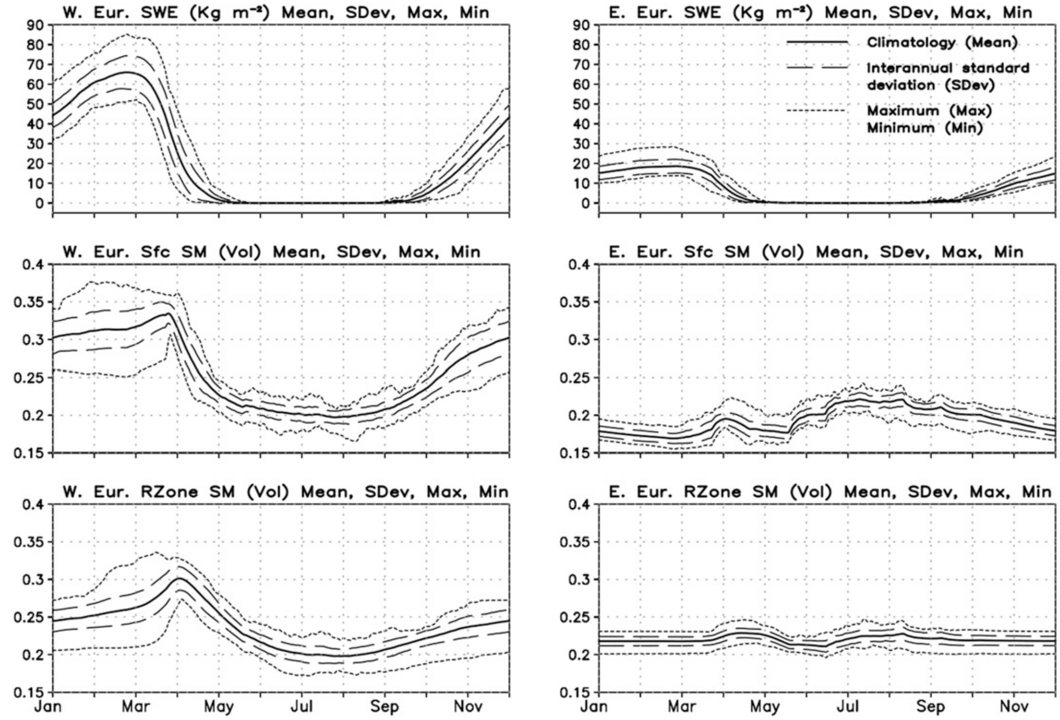

FIG. 7. Mean annual cycle of daily GLDAS-2.0 SWE (kg m^{-2}) averaged over the (top left) western Eurasia and (top right) eastern Eurasia boxes during 1967–2003. (middle), (bottom) As in (top), but for GLDAS-2.0 (middle) surface (0–10 cm) and (bottom) subsurface (10–40 cm) soil moisture. Units are volumetric. Solid line in the middle depicts the climatological mean value; long and short dashed lines depict the interannual std dev and the maximum and minimum values, respectively.

the mean sensitivity of HPBL to SHF variations during the same months is also shown (third panel of top row, Fig. 8), but based on simulations using the CFSv2 operational forecast model. The plot suggests that the atmospheric leg of coupling is also stronger over the eastern Eurasian box. Daily soil moisture anomalies composited during the POSSM and NEGSM years (bottom row, Fig. 8) suggest that, although the values are higher over the western Eurasian box during April, they decrease rapidly to almost zero by May. Hence, memory of the anomalies is also lost very soon. On the contrary, anomalies over the eastern Eurasian box, although lower in magnitude, persist longer. Therefore, despite the fact that the mean SWE, the soil moisture, and their variability are lower over the eastern Eurasian region than over the west, stronger land–atmosphere coupling creates a favorable location where surface fluxes can strongly impact the variables near the surface and in the upper atmosphere.

The modern paradigm of land–atmosphere coupling proposes that variability, strong sensitivity of surface fluxes, and long soil moisture memory should all be collocated over the same region for that region to be a strong source of land surface feedback. We support our argument about the importance of the delayed hydrological effect of eastern Eurasian snow cover using the climatological pattern of preonset soil moisture memory. Figure 9 shows the mean significant subsurface (10–40 cm below surface) soil moisture memory from GLDAS-2.0 during the premonsoon season. We estimate soil moisture memory by calculating daily lagged autocorrelations of soil moisture anomaly backward up to a lag of 90 days, starting from the onset date of monsoon in a particular year. Daily soil moisture anomaly is calculated by removing the annual cycle (sum of annual mean and first three harmonics) of each year. Significance is stringently designated when the autocorrelation falls below the 99% level of confidence. High preonset soil moisture memory is evident over the eastern part of the domain (i.e., the Tibetan Plateau), eastern Asia, and parts of northern Eurasia compared to the regions toward the west. These regions over the eastern part of Asia and Tibet are the places where the delayed snow hydrologic effect can potentially modulate the snow–atmosphere coupling strength and affect surface and atmospheric variables. Longer persistence in soil moisture anomalies over the eastern Eurasian region could also impart longer persistence in the upper-air

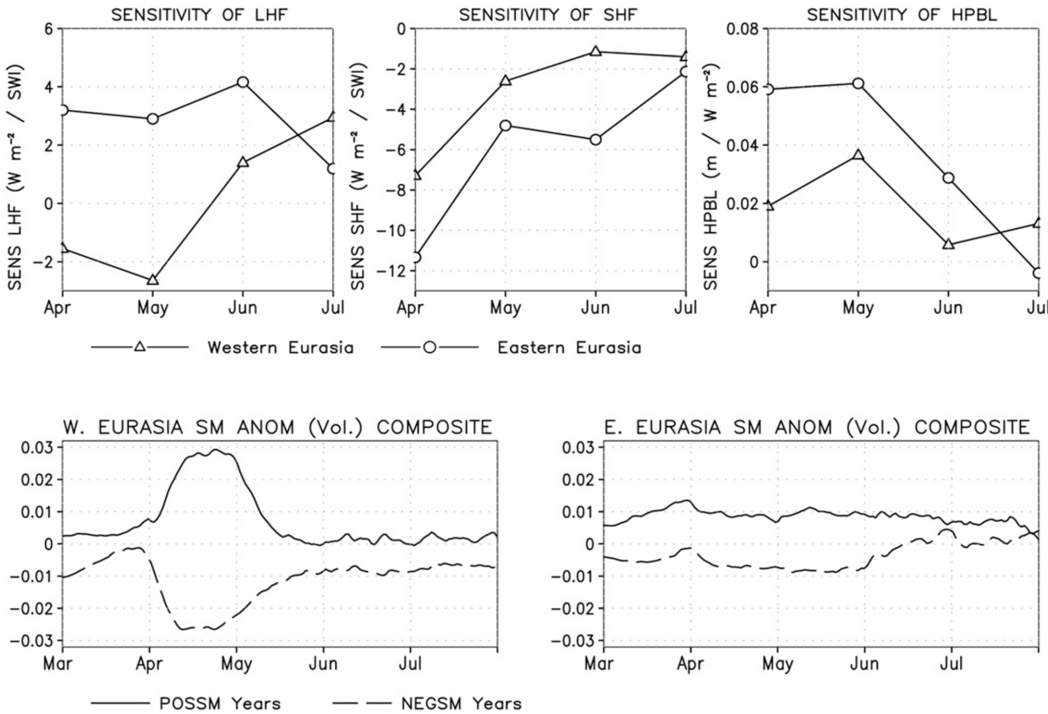

FIG. 8. (top) Mean sensitivity (SENS) of monthly (left) LHF and (middle) SHF to changes in SWI (W m^{-2} SWI^{-1}) over the western and eastern Eurasia boxes, based on GLDAS-2.0 data (1967–2003) during April–July. (right) Mean sensitivity of monthly HPBL to changes in SHF (W^{-1} m^3) based on CFSv2 model simulations (1982–2003). Sensitivity values for respective boxes are multiplied by the difference in mean monthly soil moisture anomalies (volumetric) during POSSM and NEGSM years. (bottom) Mean daily surface soil moisture anomalies (volumetric) during POSSM and NEGSM years identified from standardized anomalies of GLDAS-2.0 surface soil moisture in AM over respective boxes, during 1967–2003.

circulation anomalies around 100°E. Furthermore, we note that these are also the locations that have significant negative anomalies in SWE and soil moisture during NEGRF years over India. Soil moisture memory over the north and northwest of India during the preonset period could be associated with prolonged dry conditions or precipitation due to western disturbances generated over the Mediterranean region (Madhura et al. 2015). Detailed investigation of such events is beyond the scope of the present study. However, such evidence of long preonset soil moisture memory could be potentially utilized in improving the forecast of the monsoon onset over land through accurate land surface initialization in dynamical models (Dirmeyer and Halder 2016a).

Therefore, based on our analysis, we propose the following hypothesis. Persistence in dry soil moisture anomalies over the eastern Eurasian region during AM could help in anchoring the upper-atmospheric blocking ridge around 100°E. This, in turn, could adversely affect the Indian summer monsoon rainfall after onset through anomalous changes in the location and strength of the subtropical westerly jet and southward penetration of troughs embedded in it, as well as reduction in vertical easterly wind shear over the Indian region. It is plausible that the ''dynamical response'' evident in Fig. 5 is partly the cause for the initiation of eastern Eurasia soil moisture anomalies shown in Fig. 4 or that the circulation and soil moisture are covarying with respect to something else (e.g., SST). We have not addressed that question here, but that is a matter for investigation through modeling experiments. A schematic diagram is shown in the end (Fig. 10) in support of our proposed hypothesis. Our analysis further suggests that the snow-albedo effect is relatively more dominant (but short-lived) over the western Eurasian region, where the soil moisture memory is low. Relatively longer soil moisture memory associated with anomalous dry conditions over the eastern Eurasian region during April and May could also give us enough lead time in predicting the probability of decrease in rainfall activity on a subseasonal time scale (June and July) using operational dynamical forecast models and accurate land surface initial conditions. Validation of this hypothesis using dynamical models is being addressed in a follow-up work.

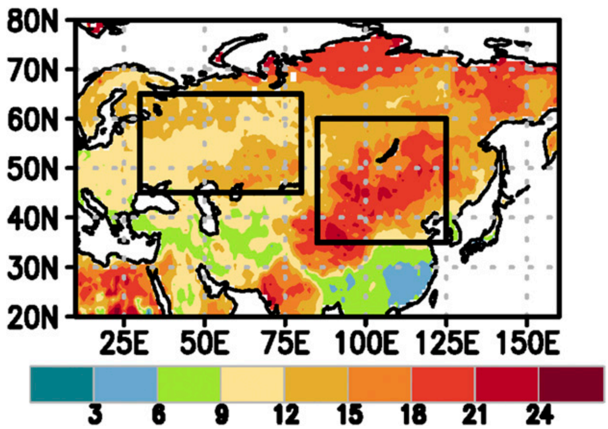

FIG. 9. Mean significant (99% confidence) GLDAS-2.0 subsurface soil moisture (10–40 cm) memory in days based on lagged autocorrelation calculated backward starting from the onset date of the Indian summer monsoon, for years 1967–2003. The western and eastern Eurasian boxes are enclosed in black lines.

4. Conclusions

Rainfall during the initial months after monsoon onset is critical for the agriculture and hydrology sectors of the Indian region, and hence its accurate forecast needs special attention. The concept of an inverse relationship between Eurasian snow cover in winter and all-India summer monsoon seasonal rainfall (during JJAS) primarily on the basis of snow-albedo effect has been investigated and demonstrated in several ways in the past [cf. Turner and Slingo (2011) and several other references in the introduction]. However, the importance of the delayed hydrological effect of snow cover over the Eurasian region in terms of the subseasonal variability of rainfall, particularly break situations, during June and July had not been explored. We propose that the delayed hydrologic impact of snowpack anomalies predominant in areas of prolonged soil moisture memory over eastern Eurasia may adversely affect rainfall after the onset of the Indian summer monsoon through changes in upper-air circulation mediated through strong land–atmosphere coupling. This study is based on observational data and observationally based reanalyses during 1967–2003.

Mean snow cover fraction (SCF) over central and northern Eurasia is stable in winter and shows variability only toward the southern edge. During this time, snow-albedo feedbacks are dominant. As snow cover over southern Eurasia starts melting in the beginning of spring, there is an increase in variability that is critical in terms of the strength of snow–atmosphere coupling. By late spring when almost all snow has melted south of 50°N, hydrological processes start to dominate the land–atmosphere feedbacks (cf. Xu and Dirmeyer 2011). The region between 50° and 70°N that has partial snow cover and snowmelt in late spring is shown to have the strongest snow–atmosphere coupling strength. The Tibetan Plateau shows strong variability during and after snowmelt because of the longer presence of snow at high altitudes. Snow water equivalent (SWE) has the potential to create this delayed snow hydrological effect and otherwise supports the spatial features shown by snow cover fraction.

There is no significant trend in all-India- or central-India-averaged rainfall during the period of observation, in either the first 30 or 60 days after onset, but there is much spatial variability over the Indian monsoon region. Based on the composite analysis of SCF and SWE using standardized anomalies of area-averaged rainfall during the first 30 and 60 days after onset, we conclude that the albedo effect is more dominant during winter (December–January and February–March), whereas the delayed hydrological effect is dominant during late spring (April–May). We infer that, during the latter part of the spring season (i.e., April–May), an increase (decrease) in SCF or SWE over northwestern (eastern) Eurasia has a negative impact on the rainfall over India during the initial 30 or 60 days after onset. In addition to that, based on the analysis of soil moisture memory and sensitivity of surface fluxes to soil moisture variations, we conclude that the delayed hydrological effect of snowmelt during April–May is more dominant over the eastern Eurasian region. The following hypothesis is proposed. A decrease in eastern Eurasian surface soil moisture during April–May is associated with an anomalous increase in surface and midtropospheric temperature, increase in midtropospheric geopotential height, and formation of an anomalous upper-level (200 hPa) ridge. Longer persistence in soil moisture anomalies and stronger land–atmosphere coupling over that region compared to the west also helps in prolonging such conditions. This upper-level anomalous anticyclone located over eastern Eurasia along with the anticyclone over Myanmar and Thailand forms a blocking ridge along 100°E that retards eastward propagation of anomalous troughs in the subtropical westerly jet. Simultaneously, these anomalous troughs embedded in the subtropical westerly jet penetrate into the Indo-Pakistan region, bringing in dry and cold air and decreasing the convective instability. The strength of the upper-level easterlies during summer decreases over the Indian region. The circulation anomalies during June and July composited on the basis of April and May eastern Eurasian soil moisture states also replicate those observed during April and May and therefore depict some level of persistence. All these dynamical and thermodynamical changes eventually lead to a decrease

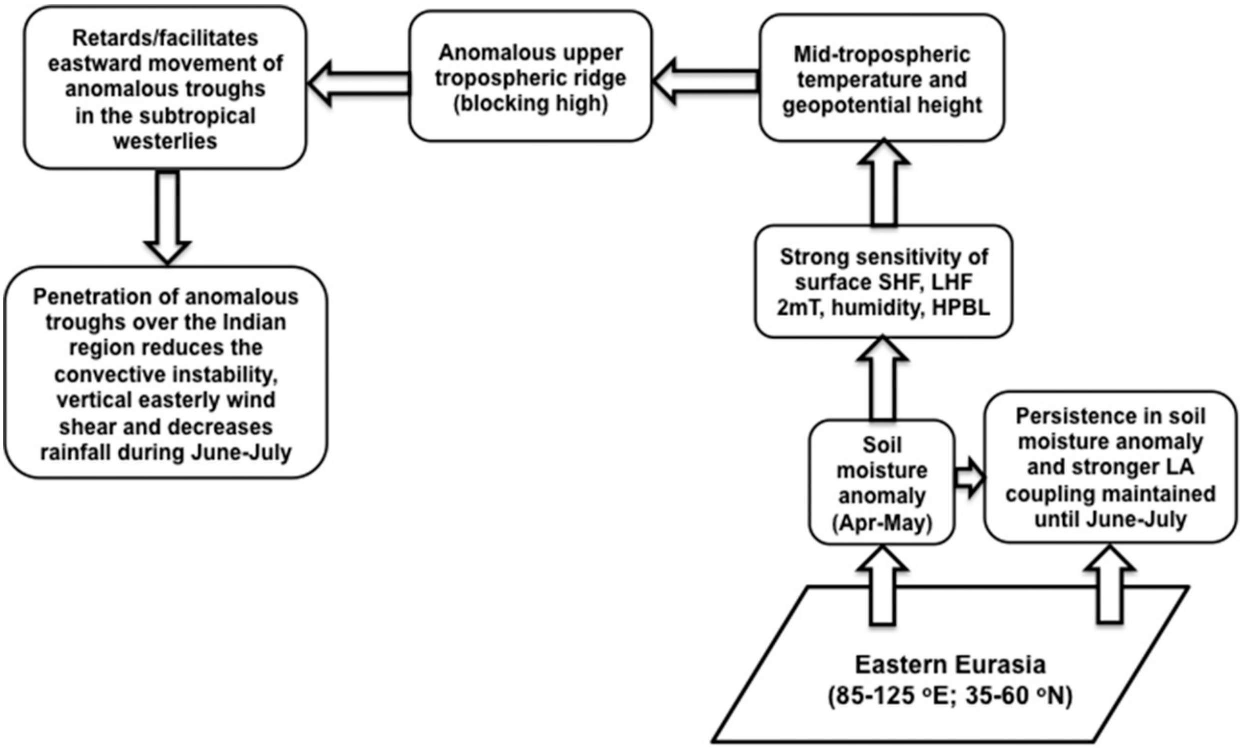

FIG. 10. Schematic diagram explaining proposed hypothesis regarding delayed hydrological effect of Eurasian snow cover and snowmelt on Indian summer monsoon rainfall after onset.

in rainfall in the post-onset period. Our analysis suggests that higher soil moisture memory over eastern Eurasia not only imparts longer persistence in the land surface states relative to western Eurasia but can also affect the upper-level circulation for a longer time, thus adversely affecting rainfall over India through teleconnections. Studies by Cohen et al. (2014) and Schubert et al. (2014) that explore how spatial variation in timing of the snowmelt or soil moisture anomalies can affect atmospheric circulation patterns also support our proposed hypothesis.

Accurate forecasts of rainfall on the subseasonal time scale (after onset) over the Indian summer monsoon region should augur well for the agriculture and hydrology sectors and also the economy of the country as a whole. For that purpose, accuracy in the prescribed snow depth, snow water equivalent, and soil moisture initial conditions and surface albedo (in both the presence and absence of snow) in an operational forecast model holds a lot of potential (Dirmeyer and Halder 2016a,b). It is also important to correctly represent physical processes related to snow and soil moisture in land surface models and parameterization of the boundary layer, radiation, convection, and clouds for better simulation of land–atmosphere feedbacks. The proposed hypothesis is being further evaluated using a comprehensive set of hindcast experiments and reanalysis data based on a state-of-the-art operational forecast model.

Acknowledgments. This research was supported by a grant from the Ministry of Earth Sciences, Government of India, under the National Monsoon Mission project. Support was also provided by grants from the National Science Foundation (AGS-1338427) and the National Aeronautics and Space Administration (NNX14AM19G) as well as a cooperative agreement with the National Oceanic and Atmospheric Administration (NA14OAR4310160). The APHRODITE precipitation is obtained from its website (http://www.chikyu.ac.jp/precip/). Monthly snow cover fraction is obtained from the Rutgers University Global Snow Lab (http://climate.rutgers.edu/snowcover/), and the methodology of its preparation is described in Robinson (1993). GLDAS-2.0 data are obtained from the Goddard Earth Sciences Data and Information Services Center (http://disc.sci.gsfc.nasa.gov/hydrology/data-holdings). For our study, 3-hourly data are converted to daily values. PBL height data came from model simulations using computational resources from the Extreme Science and Engineering Discovery Environment (XSEDE) program, as supported by National Science

Foundation Grant ACI-1053575. Specifically, we acknowledge the Texas Advanced Computing Center (TACC) at The University of Texas at Austin for providing high-performance computing resources. Those data reside on the TACC Ranch advanced storage resource.

REFERENCES

Bamzai, A. S., and J. Shukla, 1999: Relation between Eurasian snow cover, snow depth, and the Indian summer monsoon: An observational study. *J. Climate*, **12**, 3117–3112, doi:10.1175/1520-0442(1999)012<3117:RBESCS>2.0.CO;2.

——, and L. Marx, 2000: COAL AGCM simulation of the effect of anomalous spring snow over Eurasia on the Indian summer monsoon. *Quart. J. Roy. Meteor. Soc.*, **126**, 2575–2584, doi:10.1002/qj.49712656811.

Barnett, T. P., L. Dumenil, U. Schlese, and E. Roeckner, 1988: The effect of Eurasian snow cover on global climate. *Science*, **239**, 504–507, doi:10.1126/science.239.4839.504.

Blanford, H. F., 1884: On the connection of the Himalayan snowfall with dry winds and seasons of droughts in India. *Proc. Roy. Soc. London*, **37**, 3–22, doi:10.1098/rspl.1884.0003.

Buermann, W., B. Lintner, and C. Bonfils, 2005: A wintertime Arctic Oscillation signature on early season Indian Ocean monsoon intensity. *J. Climate*, **18**, 2247–2289, doi:10.1175/JCLI3377.1.

Cohen, J., and D. Rind, 1991: The effect of snow cover on the climate. *J. Climate*, **4**, 689–706, doi:10.1175/1520-0442(1991)004<0689:TEOSCO>2.0.CO;2.

——, and Coauthors, 2014: Recent Arctic amplification and extreme mid-latitude weather. *Nat. Geosci.*, **7**, 627–637, doi:10.1038/ngeo2234.

Dash, S. K., G. P. Singh, M. S. Shekhar, and A. D. Vernekar, 2005: Response of the Indian summer monsoon circulation and rainfall to seasonal snow depth anomaly over Eurasia. *Climate Dyn.*, **24**, 1–10, doi:10.1007/s00382-004-0448-3.

Delsole, T., and J. Shukla, 2012: Climate models produce skillful predictions of Indian summer monsoon rainfall. *Geophys. Res. Lett.*, **39**, L09703, doi:10.1029/2012GL051279.

Dey, B., and O. S. R. U. Bhanukumar, 1982: An apparent relationship between Eurasian spring snow cover and the advance period of the Indian summer monsoon. *J. Appl. Meteor.*, **21**, 1929–1932, doi:10.1175/1520-0450(1982)021<1929:AARBES>2.0.CO;2.

——, S. N. Kathuria, and O. B. Kumar, 1985: Himalayan summer snow cover area and withdrawal of the Indian summer monsoon. *J. Climate Appl. Meteor.*, **24**, 865–868, doi:10.1175/1520-0450(1985)024<0865:HSSCAW>2.0.CO;2.

Dickinson, R. E., 1983: Land surface processes and climate—Surface albedos and energy balance. *Advances in Geophysics*, Vol. 25, Academic Press, 305–353, doi:10.1016/S0065-2687(08)60176-4.

Dickson, R. R., 1984: Eurasian snow cover versus Indian monsoon rainfall—An extension of the Hahn–Shukla results. *J. Climate Appl. Meteor.*, **23**, 171–173, doi:10.1175/1520-0450(1984)023<0171:ESCVIM>2.0.CO;2.

Dirmeyer, P. A., 2011: The terrestrial segment of soil moisture–climate coupling. *Geophys. Res. Lett.*, **38**, L16702, doi:10.1029/2011GL048268.

——, and S. Halder, 2016a: Sensitivity of numerical weather forecasts to initial soil moisture variations in CFSv2. *Wea. Forecasting*, **31**, 1973–1983, doi:10.1175/WAF-D-16-0049.1.

——, and ——, 2016b: Application of the land–atmosphere coupling paradigm to the operational Coupled Forecast System (CFSv2). *J. Hydrometeor.*, **18**, 85–108, doi:10.1175/JHM-D-16-0064.1.

——, Z. Wang, M. J. Mbuh, and H. E. Norton, 2014: Intensified land surface control on boundary layer growth in a changing climate. *Geophys. Res. Lett.*, **41**, 1290–1294, doi:10.1002/2013GL058826.

Dong, B., and P. J. Valdes, 1998: Modelling the Asian summer monsoon rainfall and Eurasian winter/spring snow mass. *Quart. J. Roy. Meteor. Soc.*, **124**, 2567–2596, doi:10.1002/qj.49712455203.

Douville, H., 2010: Relative contribution of soil moisture and snow mass to seasonal climate predictability: A pilot study. *Climate Dyn.*, **34**, 797–818, doi:10.1007/s00382-008-0508-1.

——, and J.-F. Royer, 1996: Sensitivity of the Asian summer monsoon to an anomalous Eurasian snow cover within the Météo-France GCM. *Climate Dyn.*, **12**, 449–466, doi:10.1007/BF02346818.

Ek, M. B., K. E. Mitchell, Y. Lin, E. Rogers, P. Grunmann, V. Koren, G. Gayno, and J. D. Tarpley, 2003: Implementation of Noah land surface model advances in the National Centers for Environmental Prediction operational mesoscale Eta model. *J. Geophys. Res.*, **108**, 8851, doi:10.1029/2002JD003296.

Fasullo, J., 2004: A stratified diagnosis of the Indian monsoon–Eurasian snow cover relationship. *J. Climate*, **17**, 1110–1122, doi:10.1175/1520-0442(2004)017<1110:ASDOTI>2.0.CO;2.

Ferranti, L., and F. Molteni, 1999: Ensemble simulations of Eurasian snow-depth anomalies and their influence on the summer Asian monsoon. *Quart. J. Roy. Meteor. Soc.*, **125**, 2597–2610, doi:10.1002/qj.49712555913.

Gong, G., D. Entekhabi, J. Cohen, and D. Robinson, 2004: Sensitivity of atmospheric response to modeled snow anomaly characteristics. *J. Geophys. Res.*, **109**, D06107, doi:10.1029/2003JD004160.

Goswami, B. N., 2007: South Asian monsoon. *Intraseasonal Variability in the Atmosphere–Ocean Coupled System*, 1st ed. W. K. M. Lau and D. Waliser, Eds., Springer, 21–72, doi:10.1007/978-3-642-13914-7.

——, and P. K. Xavier, 2005: Dynamics of ''internal'' interannual variability of Indian summer monsoon in a GCM. *J. Geophys. Res.*, **110**, D24104, doi:10.1029/2005JD006042.

Griffies, S. M., M. J. Harrison, R. C. Pacanowski, and A. Rosati, 2004: A Technical Guide to MOM4. GFDL Ocean Group Tech. Rep. 5, 281 pp.

Hahn, D. G., and J. Shukla, 1976: An apparent relationship between the Eurasian snow cover and Indian monsoon rainfall. *J. Atmos. Sci.*, **33**, 2461–2462, doi:10.1175/1520-0469(1976)033<2461:AARBES>2.0.CO;2.

Halder, S., P. A. Dirmeyer, and S. K. Saha, 2015: Sensitivity of the mean and variability of Indian summer monsoon to land surface schemes in RegCM4: Understanding coupled land–atmosphere feedbacks. *J. Geophys. Res.*, **120**, 9437–9458, doi:10.1002/2015JD023101.

——, S. K. Saha, P. A. Dirmeyer, T. N. Chase, and B. N. Goswami, 2016: Investigating the impact of land-use land-cover change on Indian summer monsoon daily rainfall and temperature during 1951–2005 using a regional climate model. *Hydrol. Earth Syst. Sci.*, **20**, 1765–1784, doi:10.5194/hess-20-1765-2016.

Hall, A., X. Qu, and J. D. Neelin, 2008: Improving predictions of summer climate change in the United States. *Geophys. Res. Lett.*, **35**, L01702, doi:10.1029/2007GL032012.

Harris, I., P. D. Jones, T. J. Osborn, and D. H. Lister, 2014: Updated high-resolution grids of monthly climatic observations—The CRU TS3.10 dataset. *Int. J. Climatol.*, **34**, 623–642, doi:10.1002/joc.3711.

Jiang, X., T. Li, and B. Wang, 2004: Structures and mechanisms of the northward propagating boreal summer intraseasonal oscillations. *J. Climate*, **17**, 1022–1039, doi:10.1175/1520-0442(2004)017<1022:SAMOTN>2.0.CO;2.

Khandekar, M. L., 1991: Eurasian snow cover, Indian monsoon and El Niño/Southern Oscillation—A synthesis. *Atmos.–Ocean*, **29**, 636–647, doi:10.1080/07055900.1991.9649422.

Koster, R.D., and Coauthors, 2004: Regions of strong coupling between soil moisture and precipitation. *Science*, **305**, 1138–1140, doi:10.1126/science.1100217.

Kothawale, D. R., and J. R. Kulkarni, 2014: Performance of all-India southwest monsoon seasonal rainfall when monthly rainfall reported as deficit/excess. *Meteor. Appl.*, **21**, 619–634, doi:10.1002/met.1385.

Kripalani, R. H., and A. Kulkarni, 1999: Climatology and variability of historical Soviet snow depth data: Some new perspectives in snow–Indian monsoon teleconnections. *Climate Dyn.*, **15**, 475–489, doi:10.1007/s003820050294.

Krishnamurthy, V., and J. Shukla, 2000: Intraseasonal and interannual variability of rainfall over India. *J. Climate*, **13**, 4366–4377, doi:10.1175/1520-0442(2000)013<0001:IAIVOR>2.0.CO;2.

Krishnan, R., C. Zhang, and M. Sugi, 2000: Dynamics of breaks in the Indian summer monsoon. *J. Atmos. Sci.*, **57**, 1354–1372, doi:10.1175/1520-0469(2000)057<1354:DOBITI>2.0.CO;2.

——, V. Kumar, M. Sugi, and J. Yoshimura, 2009: Internal feedbacks from monsoon–midlatitude interactions during droughts in the Indian summer monsoon. *J. Atmos. Sci.*, **66**, 553–578, doi:10.1175/2008JAS2723.1.

Kumar, K. K., and Coauthors, 2011: The once and future pulse of Indian summer monsoon. *Climate Dyn.*, **36**, 2159–2170, doi:10.1007/s00382-010-0974-0.

Madhura, R. K., R. Krishnan, J. V. Revadekar, M. Mujumdar, and B. N. Goswami, 2015: Changes in western disturbances over the western Himalayas in a warming environment. *Climate Dyn.*, **44**, 1157–1168, doi:10.1007/s00382-014-2166-9.

Meehl, G., 1994: Coupled land–ocean–atmosphere processes and South Asian monsoon variability. *Science*, **266**, 263–267, doi:10.1126/science.266.5183.263.

Niu, G.-Y., and Z.-L. Yang, 2006: Effects of frozen soil on snowmelt runoff and soil water storage at a continental scale. *J. Hydrometeor.*, **7**, 937–952, doi:10.1175/JHM538.1.

Pai, D. S., and M. Rajeevan, 2009: Summer monsoon onset over Kerala: New definition and prediction. *J. Earth Syst. Sci.*, **118**, 123–135, doi:10.1007/s12040-009-0020-y.

Parthasarathy, B., and S. Yang, 1995: Relationships between regional Indian summer monsoon rainfall and Eurasian snow cover. *Adv. Atmos. Sci.*, **12**, 143–150, doi:10.1007/BF02656828.

Peings, Y., and H. Douville, 2010: Influence of the Eurasian snow cover on the Indian summer monsoon variability in observed climatologies and CMIP3 simulations. *Climate Dyn.*, **34**, 643–660, doi:10.1007/s00382-009-0565-0.

Rai, A., S. K. Saha, S. Pokhrel, K. Sujith, and S. Halder, 2015: Influence of preonset land atmospheric conditions on the Indian summer monsoon rainfall variability. *J. Geophys. Res.*, **120**, 4551–4563, doi:10.1002/2015JD023159.

Robinson, D. A., 1993: Monitoring Northern Hemisphere snow cover. Snow watch '92: Detection strategies for snow and ice, National Snow and Ice Data Center Glaciological Data Rep. GD-25, 1–25. [Available online at https://nsidc.org/pubs/documents/gd/GD-25_web.pdf.]

——, and A. Frei, 2000: Seasonal variability of Northern Hemisphere snow extent using visible satellite data. *Prof. Geogr.*, **52**, 307–315, doi:10.1111/0033-0124.00226.

Robock, A., M. Mu, K. Vinnikov, and D. Robinson, 2003: Land surface conditions over Eurasia and Indian summer monsoon rainfall. *J. Geophys. Res.*, **108**, 4131, doi:10.1029/2002JD002286.

Rodell, M., and Coauthors, 2004: The Global Land Data Assimilation System. *Bull. Amer. Meteor. Soc.*, **85**, 381–394, doi:10.1175/BAMS-85-3-381.

Ropelewski, C. F., A. Robock, and M. Matson, 1984: Comments on "An apparent relationship between the Eurasian snow cover and Indian monsoon rainfall." *J. Climate Appl. Meteor.*, **23**, 341–342, doi:10.1175/1520-0450(1984)023<0341:COARBE>2.0.CO;2.

Saha, S., and Coauthors, 2010: The NCEP Climate Forecast System Reanalysis. *Bull. Amer. Meteor. Soc.*, **91**, 1015–1057, doi:10.1175/2010BAMS3001.1.

——, and Coauthors, 2014: The NCEP Climate Forecast System version 2. *J. Climate*, **27**, 2185–2208, doi:10.1175/JCLI-D-12-00823.1.

Saha, S. K., S. Halder, K. K. Kumar, and B. N. Goswami, 2011: Pre-onset land surface processes and 'internal' interannual variabilities of the Indian summer monsoon. *Climate Dyn.*, **36**, 2077–2089, doi:10.1007/s00382-010-0886-z.

——, ——, A. S. Rao, and B. N. Goswami, 2012: Modulation of ISOs by land–atmosphere feedback and contribution to the interannual variability of the Indian summer monsoon. *J. Geophys. Res.*, **117**, D13101, doi:10.1029/2011JD017291.

——, S. Pokhrel, and H. S. Chaudhari, 2013: Influence of Eurasian snow on Indian summer monsoon in NCEP CFSv2 freerun. *Climate Dyn.*, **41**, 1801–1815, doi:10.1007/s00382-012-1617-4.

Sahai, A. K., R. Chattopadhyay, S. Joseph, R. Mandal, A. Dey, S. Abhilash, R. P. M. Krishna, and N. Borah, 2015: Real-time performance of a multi-model ensemble-based extended range forecast system in predicting the 2014 monsoon season based on NCEP-CFSv2. *Curr. Sci.*, **109**, 1802–1813, doi:10.18520/v109/i10/1802-1813.

Samanta, D., M. K. Dash, B. N. Goswami, and P. C. Pandey, 2015: Extratropical anticyclonic Rossby wave breaking and Indian summer monsoon failure. *Climate Dyn.*, **46**, 1547–1562, doi:10.1007/s00382-015-2661-7.

Sankar-Rao, M., K. M. Lau, and S. Yang, 1996: On the relationship between Eurasian snow cover and the Asian summer monsoon. *Int. J. Climatol.*, **16**, 605–616, doi:10.1002/(SICI)1097-0088(199606)16:6<605::AID-JOC41>3.0.CO;2-P.

Schubert, S. D., H. Wang, R. D. Koster, and M. J. Suarez, 2014: Northern Eurasian heat waves and droughts. *J. Climate*, **27**, 3169–3207, doi:10.1175/JCLI-D-13-00360.1.

Senan, R., and Coauthors, 2016: Impact of springtime Himalayan–Tibetan Plateau snowpack on the onset of the Indian summer monsoon in coupled seasonal forecasts. *Climate Dyn.*, **47**, 2709–2725, doi:10.1007/s00382-016-2993-y.

Shinoda, M., 2001: Climate memory of snow mass as soil moisture over central Eurasia. *J. Geophys. Res.*, **106**, 33 393–33 403, doi:10.1029/2001JD000525.

Shukla, J., 1984: Predictability of time averages. Part II: The influence of the boundary forcing. *Problems and Prospects in Long and Medium Range Weather Forecasting*, D. M. Burridge and E. Kallen, Eds., Topics in Atmospheric and Oceanographic Sciences, Springer-Verlag, 155–206, doi:10.1007/978-3-642-82132-5_6.

——, and D. A. Mooley, 1987: Empirical prediction of the summer monsoon rainfall over India. *Mon. Wea. Rev.*, **115**, 695–703, doi:10.1175/1520-0493(1987)115<0695:EPOTSM>2.0.CO;2.

Sikka, D. R., and S. Gadgil, 1980: On the maximum cloud zone and the ITCZ over Indian longitudes during the southwest monsoon. *Mon. Wea. Rev.*, **108**, 1840–1853, doi:10.1175/1520-0493(1980)108<1840:OTMCZA>2.0.CO;2.

Soman, M. K., and K. Krishna Kumar, 1993: Space-time evolution of meteorological features associated with the onset of Indian summer monsoon. *Mon. Wea. Rev.*, **121**, 1177–1194, doi:10.1175/1520-0493(1993)121<1177:STEOMF>2.0.CO;2.

Thompson, D. W. J., and J. M. Wallace, 2000: Annular modes in the extratropical circulation. Part I: Month-to-month variability. *J. Climate*, **13**, 1000–1016, doi:10.1175/1520-0442(2000)013<1000:AMITEC>2.0.CO;2.

Turner, A. G., and J. M. Slingo, 2011: Using idealized snow forcing to test teleconnections with the Indian summer monsoon in the Hadley Center GCM. *Climate Dyn.*, **36**, 1717–1735, doi:10.1007/s00382-010-0805-3.

Uppala, S. M., and Coauthors, 2005: The ERA-40 Re-Analysis. *Quart. J. Roy. Meteor. Soc.*, **131**, 2961–3012, doi:10.1256/qj.04.176.

Vernekar, A. D., J. Zhou, and J. Shukla, 1995: The effect of Eurasian snow cover on the Indian monsoon. *J. Climate*, **8**, 248–266, doi:10.1175/1520-0442(1995)008<0248:TEOESC>2.0.CO;2.

Walland, D. J., and I. Simmonds, 1996: Modelled atmospheric response to changes in Northern Hemisphere snow cover. *Climate Dyn.*, **13**, 25–34, doi:10.1007/s003820050150.

Webster, P. J. and S. Yang, 1992: Monsoon and ENSO: Selectively interactive systems. *Quart. J. Roy. Meteor. Soc.*, **118**, 877–926, doi:10.1002/qj.49711850705.

Wiscombe, W. J., and S. G. Warren, 1980: A model for the spectral albedo of snow. I: Pure snow. *J. Atmos. Sci.*, **37**, 2712–2733, doi:10.1175/1520-0469(1980)037<2712:AMFTSA>2.0.CO;2.

Xu, L., and P. Dirmeyer, 2011: Snow–atmosphere coupling strength in a global atmospheric model. *Geophys. Res. Lett.*, **38**, L13401, doi:10.1029/2011GL048049.

——, and ——, 2013a: Snow–atmosphere coupling strength. Part I: Effect of model biases. *J. Hydrometeor.*, **14**, 389–403, doi:10.1175/JHM-D-11-0102.1.

——, and ——, 2013b: Snow–atmosphere coupling strength. Part II: Albedo effect versus hydrological effect. *J. Hydrometeor.*, **14**, 404–418, doi:10.1175/JHM-D-11-0103.1.

——, H. Gao, and Y.-Q. Li, 2009: Sensible heating over the Tibetan Plateau linked to the onset of Asian monsoon. *Atmos. Oceanic Sci. Lett.*, **2**, 350–356, doi:10.1080/16742834.2009.11446833.

Yang, S., 1996: ENSO–snow–monsoon associations and seasonal–interannual predictions. *Int. J. Climatol.*, **16**, 125–134, doi:10.1002/(SICI)1097-0088(199602)16:2<125::AID-JOC999>3.0.CO;2-V.

Yatagai, A., K. Kamiguchi, O. Arakawa, A. Hamada, N. Yasutomi, and A. Kitoh, 2012: APHRODITE: Constructing a long-term daily gridded precipitation dataset for Asia based on a dense network of rain gauges. *Bull. Amer. Meteor. Soc.*, **93**, 1401–1415, doi:10.1175/BAMS-D-11-00122.1.